ISTITUTO NAZIONALE DI FISICA NUCLEARE

LABORATORI NAZIONALI DI FRASCATI

Proposal to search for a dark photon in e[+] on target collisions at DAFNE linac

M. Raggi[1], V. Kozhuharov[1,2]

[1] *INFN- LNF, v. E. Fermi, 40, 00044 Laboratori Frascati (Roma), Italy*
[2] *University of Sofia "St. Kl. Ohridski", Sofia, Bulgaria*

Abstract

Photon-like particles are predicted in many extensions of the Standard Model. They have interactions similar to the photon, are vector bosons, and can be produced together with photons. The present paper proposes a search for such particles in the $e^+e- \rightarrow Ug$ process in a positron-on-target experiment, exploiting the positron beam of the DAFNE LINAC at the Laboratori Nazionali di Frascati, INFN.

With a 550 MeV/c beam and 10^4 positrons per bunch in one year of running a sensitivity in the relative coupling constant down to 10^{-6}

is achievable, in the mass region from 2.5 MeV $< M_U <$ 20 MeV, compatible with the preferred region from the 3s discrepancy in g_m -2. The proposed experimental setup and the analysis technique is discussed.

1   Introduction

Since the first data from LHC have given no evidence of new degrees of freedom at the highest energies explored nowadays, the unexplained nature of the dark matter remains one of the best places to look for Standard Model extensions. A recent approach to explain the unobserved dark matter is the concept of a hidden sector. Since the interactions of such sectors with the visible one can be very weak, so are the current experimental bounds. Therefore hidden sectors might even contain sub-GeV-scale particles that have so far escaped detection.

The results by PAMELA in 2008 on the positron excess [1], recently confirmed by FERMI [2] and AMS[3], have give rise to interest on dark matter candidates. A possible mechanism for generating such an excess is the dark matter annihilation process into a new particle, a messenger connecting the visible with the invisible sector, which afterwards decays into a e^+e^- pair. The observation of no excess in the anti-proton to proton flux again by PAMELA [4] suggests that these messengers must be lighter than $\sim 1\ GeV$ or that they decay mainly into leptons. The same kind of particles can even contribute, through loop diagrams, to $g_\mu - 2$, explaining the present 3σ discrepancy with respect to the Standard Model prediction [5].

The simplest hidden sector model just introduces one extra U(1) gauge symmetry and a corresponding gauge boson: the "dark photon" or U boson. As in QED, this will generate interactions of the types

$$\mathcal{L} \sim g' q_f \bar{\psi}_f \gamma^\mu \psi_f U'_\mu, \tag{1}$$

where g' is the universal coupling constant of the new interaction and q_f are the corresponding charges of the interacting fermions. Not all the Standard Model particles need to be charged under this new U(1) symmetry thus leading in general to a different (and sometimes vanishing) interaction strength for quarks and leptons. In the case of zero U(1) charge of the quarks [6], the new gauge boson cannot be directly produced in hadron collisions or meson decays.

The coupling constant and the charges can result from a direct interaction between the Standard Model fermions and the new gauge fields or can be generated effectively through the so called kinetic mixing mechanism between the QED and the new U(1) gauge bosons [7]. In the latter case the charges q_f in eq.(1) will be just proportional to the electric charge and the associated mixing term in the QED Lagrangian will be

$$\mathcal{L}_{mix} = -\frac{\epsilon}{2} F^{QED}_{\mu\nu} F^{\mu\nu}_{dark}. \tag{2}$$

The associated mixing coupling constant, ϵ, can be so small ($< 10^{-3}$) as to preclude the discovery of the dark photon in most of the experiments carried out so far. Another possibility is mass mixing with the Z, in which case the particle could also posses Z-like properties.

In the hypothesis that the dark sector does not contain any particle of mass lower than that of the U boson, and that M_U is smaller than twice the muon mass, the U can only decay to e^+e^- pairs. In this hypothesis, the U is expected to be a very narrow resonance whose total decay width is given by:

$$\Gamma_U = \Gamma_{U \to e+e-} = \frac{1}{3}\alpha\epsilon^2 M_U \sqrt{1 - \frac{4me^2}{M_U^2}}\left(1 + \frac{2me^2}{M_U^2}\right) \tag{3}$$

which leads to a lifetime τ_U which is proportional to $1/(\epsilon^2 M_U)$.

In general, a hypothetical vector particle within the MeV-GeV mass range acting as a gauge boson and a messenger to a hidden sector could possibly be part of the understanding of two unexplained phenomena within the Standard Model and is predicted in many of its extensions. The present article describes a proposal devoted to the search for such a particle in a positron on target experiment.
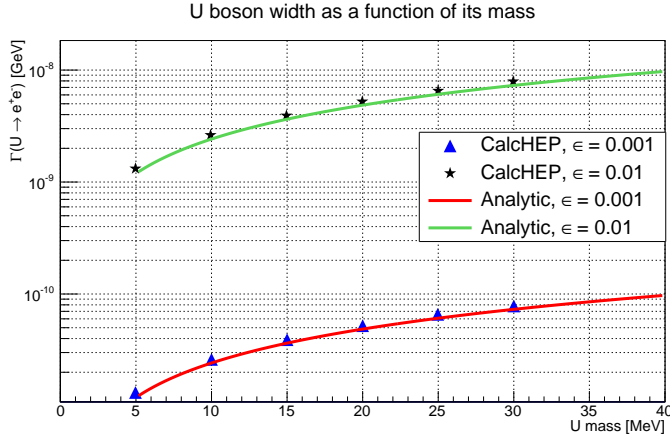
Figure 1: U boson width calculated with formula 3 and compared to the toy model implemented in CalcHEP. Matching between the different calculation is better than 10%.

To be able to simulate the production of the U boson, the Lagrangian term from formula (1), assuming $\psi = e$, was implemented in the CalcHEP [8] simulation software with $g'q_f = \epsilon$. The results obtained for the decay width $\Gamma_{U \to e+e-}$ as a function of the U boson mass were compared with the analytic formula (3) and are shown in Figure 1 for two different values of ϵ. The difference between analytic and simulated values is less than 15%, allowing the usage of CalcHEP for our studies. In this notation the ratio of the strengths of the electromagnetic (α) and the new U(1) (α') interactions is $\alpha'/\alpha = \epsilon^2$.

2 Present status of experimental searches

Many searches have been performed in recent years to detect low energy exotic particles like the U boson exploiting different techniques that can be divided into three groups:

- Direct searches in beam dump experiments

- Fixed target experiments

- Direct searches in decays of mesons like π^0, η, ϕ, Υ

Based on the final state the experiment is looking at, the searches can also be divided into visible and invisible. Visible searches implement a full reconstruction of the U boson decay products, usually e^+e^- or $\mu^+\mu^-$ and are thus less demanding in terms of the definition of the initial-state kinematics. However, the presence of a well defined initial state helps to reduce the background. The invisible searches do not assume that the U boson decay products, if any, are detectable by the experiment. However, if there are no Standard Model particles in the final state, a more stringent limit could be obtained through more efficient background vetoing. Both types of searches are complementary and are equally important.

The limits on U boson searches from beam dump experiments come from reanalysis [9] of a compete set of experiments performed at SLAC and Fermilab during the '80s and '90s to search for light Axion-like particles [10, 11, 12]. These studies were triggered by the the observation of a 1.8 MeV mono-energetic positron peak in heavy-ion collisions at GSI in 1983 [13]. In these experiments, U bosons or axion like particles are produced, with a process similar to bremsstrahlung

of ordinary photons, by a very intense electron beam incident on a dump. The produced particles travel through the dump due to their long lifetime and are observed by a detector behind the dump through their decays into e^+e^- pairs. In this kind of experiment, the measured quantity is in fact $\epsilon^2 \cdot BR(U \to e^+e^-)$. If in the dark sector no particle lighter than the electron exists the limits are valid; otherwise the U boson will decay into this new particle and may remain undetected in the experiment.

The main advantage of this approach is the huge luminosity, beam flux up to 10^{10} particle/s, and the high cross section due to the use of a target of high-Z material. Since the beam is completely absorbed in the dump, no events are observed and the limits scale with the number of primaries. On the other hand the sensitivity is limited, in the U boson case, to an interval of small values of ϵ^2. The dump thickness sets the minimum lifetime of observable U bosons, and hence the maximum observable ϵ. On the other hand, for ϵ smaller than a certain value, the U bosons live so long that most decay outside the detector acceptance. Finally the mass range probed is limited by the beam energy due to the $1/E^2$ probability to radiate a high energy γ^*. In Figure 2 the present limits for dump experiments are shown in gray in the leftmost part.

Fixed target experiments share the same beam type and production mechanism as dump experiments. The e^+e^- invariant mass spectrum is searched for narrow resonances. The thickness of the target is reduced in order to allow short living U-boson to escape. The angular coverage of the spectrometer limits the acceptance and the accessible mass region. The exclusions from MAMI[14] and APEX[15] experiments are shown in Figure 2.
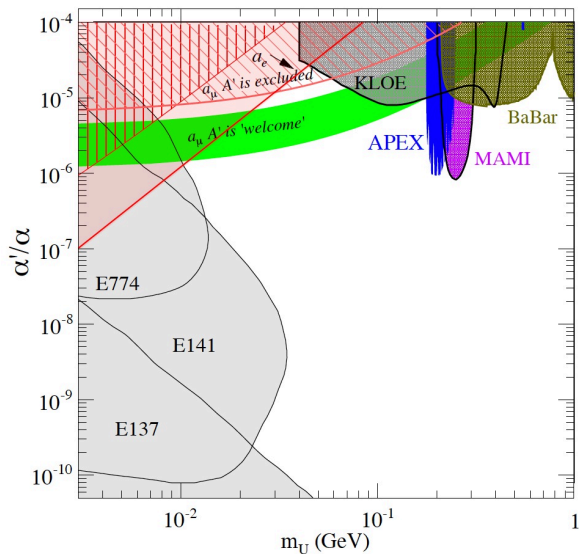

Figure 2: *Exclusion region in the hypothesis of decay into lepton pairs*
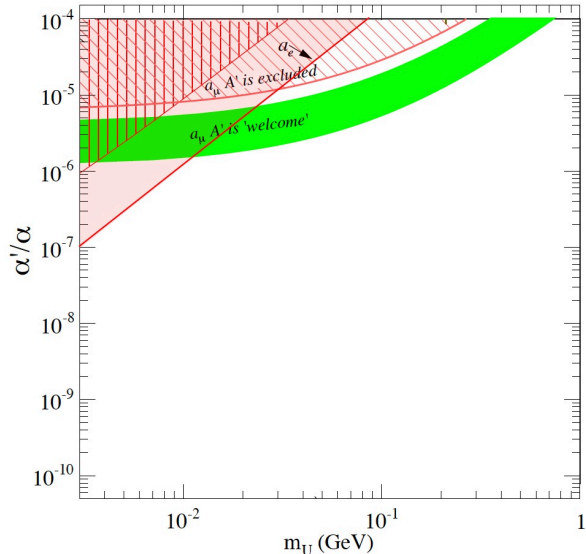
Figure 3: *Exclusion region in the hypothesis of decay to invisible.*

Collider experiments have searched for resonances in the e^+e^- ($\mu^+\mu^-$) mass spectra [16] for the decay products of mesons like π^0, η, ϕ or Υ. Searches of this kind have been performed by WASA-at-COSY[17], KLOE[18, 19] and BaBar[20]. They are limited in mass reach by the mass of the meson or they assume that the U boson couples to quarks and to leptons with the same strength and that it decays into lepton pairs. The advantage of this approach is the ability to investigate the high mass region, up to ~ 1 GeV, and very short lifetimes inaccessible to beam dump experiments. On the other hand, the number of particles produced is smaller in this kind

of experiment with respect to a fixed target experiment. The difference can be as high as a factor 1000. The results from collider experiments are shown in the top right part of Figure 2.

The U boson would also cotribute to the anomalous magnetic moments of the electron and muon. The contribution can be written as [21]

$$a = \frac{g-2}{2}; \; \Delta a = \frac{\alpha \epsilon^2}{2\pi} \times f, \tag{4}$$

where α is the fine structure constant, $f = 1$ for $m_l \gg M_U$ and $f = 2m_l^2/(3M_U^2)$ for $m_l \ll M_U$. At present, α is in fact determined from the measurement of the electron magnetic moment g_e [22] and then is used to calculate the muon anomalous magnetic moment. Comparison between the theoretical and the experimental value allows a limit to be set in the $M_U - \epsilon^2$ parameter space, shown with diagonal stripes in Figure 2. On the contrary the well known 3σ discrepancy between the measured value of g_μ and the Standard Model prediction [5] can be explained by the existence of the U boson. In this hypothesis a band of mass coupling values, in green in Figure 2, is identified. This region is of particular interest and is not thoroughly explored at present.

An external knowledge of α is necessary to exploit the measurement of g_e to set limits on the U boson parameters. The fine structure constant was extracted from a recent single measurement of the ratio between the Planck constant and the mass of the ^{87}Rb atom [23]. The precision achieved is an order of magnitude better than that for the previous measurements, which had been conducted two years earlier. That measurement, combined with equation (4) and the latest tenth-order calculations of the QED contributions [24] to g_e, gives a bound, shown by the pink line in Figure 2, reaching $\epsilon^2 < 10^{-7}$ for $M_U = 1 MeV$ and $\epsilon^2 < 10^{-4}$ for $M_U = 100 MeV$. The limits from the measurements before [23] are also shown in vertical stripes.

There are no results at present from searches for invisible decays. The only limits on the M_U and ϵ are from the previously described magnetic moment measurements. The scenario is illustrated in Figure 3. Since even the preferred by $(g_\mu - 2)$ region is not completely covered, new experiments devoted to the the search for U boson are highly desirable.

3 Beam Test Facility at LNF

The DAΦNE beam-test facility (BTF), shown in Figure 4, is a beam transfer-line [25] capable of providing bunches of electrons and positrons from the DAΦNE linac. It is generally operated for injection into the storage rings of the DAΦNE phi-factory. The DAΦNE linac is a S-band linear accelerator, made up of travelling-wave constant-gradient units fed by SLED-compressed RF pulses. It is capable of providing electrons or positrons, up to 50 bunches per second, generally of energy 510 MeV and 10 ns time duration, optimized for the operation of the e^+e^- collider at the ϕ meson resonance. The RF power is provided by four 45 MW klystrons. The Linac is composed of two parts: the low-energy, high-current first section, from the thermo-ionic gun to the positron converter, made up of five accelerating structures, fed by the A and B klystrons, and the high-energy, low current final section, made up of ten accelerating structures, two fed by the A klystron, and four each fed by the C and D klystrons. The maximum achievable energy for electrons/positrons is then 800/550 MeV. The minimum energy at which the Linac can be operated is below 250 MeV both in electron and positron mode, even though some optimization is necessary in order to obtain stable and safe operation. An energy upgrade of the Linac is foreseen within the next three years [26], by adding a fifth power station (modulator, 45 MW klystron and SLED), bringing the maximum energy for electrons/positrons to about 1050/800 MeV. The typical emittance of the electron/positron beam is of 1(1.5) mm*mrad, while the maximum beam current is of 500 mA (100 mA). Beam characteristics
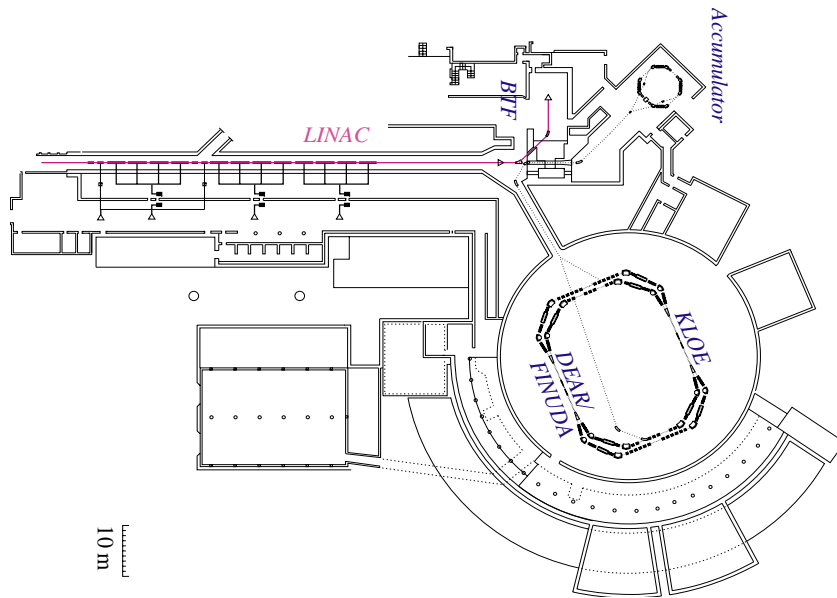
Figure 4: Layout of the DAΦNE complex at Laboratori Nazionali di Frascati, INFN

	e^+	e^-	e^+_{Upg}	e^-_{Upg}
Maximal beam energy [MeV]	550	800	800	1050
Beam rate [particles/bunch]	$6.2 \cdot 10^8$	$6.2 \cdot 10^8$	$6 \cdot 10^9$	$3.1 \cdot 10^{10}$
Number of bunch per second	50	50	50	50
Max. averaged current during a bunch [mA]	10	10	100	500
Typical emittance (mm mrad)	1.5	1.	1.5	1.
Beam spot size (σ in mm)	2.	2.	2.	2.

Table 1: BTF beam parameters [25]. A possible increase of the performance after an upgrade is also shown

(spot size, divergence, momentum resolution), strongly depend on the beam energy and the number of particles per bunch. The parameters are summarized in Table 1. Any of the 50 Linac bunches can be injected to the Damping Ring, and from there to the DAΦNE main rings, or extracted (by a pulsed magnet) to the BTF beam line, where the electron or positron beam can be attenuated by means of a variable-depth copper target and further energy selected or simply transported to an experimental beam hall. The beam energy selection is performed by a 42 degree bending magnet plus horizontal tungsten collimators; the momentum can be defined with an accuracy of better than 1%. In normal operation, one of the 50 pulses/second is sent to a magnetic spectrometer for a precise measurement of the beam momentum. Presently, the maximum beam intensity in the BTF experimental hall is limited by radio-protection safety regulations at $3.12 \cdot 10^{10}$ particles/second.

The BTF beam-line has been used for more than ten years by many experimental groups, mainly for detector testing purposes, thanks to the possibility of delivering a finely tuned beam attenuated down to single-particle intensity, with a definite energy (down to few tens of MeV), a well defined beam spot (2 mm sigma both in x and y), and a small divergence (below 2 mrad). It

is also (occasionally) used at the maximum allowed intensity.

In the present configuration, the BTF line comprises four quadrupoles for adjusting the beam optics and an additional set of vertical and horizontal tungsten slits for collimation. In the experimental hall, particles can be either delivered on a straight beam line, or deflected by 45 degrees by a dipole magnet. The entire BTF line is operated in the Linac high vacuum, but can be easily disconnected from it: it is equipped with safety vacuum valves and a dedicated vacuum pump. The most important limitation of the linac for the project described in this paper is the very short duration of the bunch, 10 ns, and the 50 bunches/s delivered. In fact, to obtain a sufficiently high event rate a high number of e^+ per bunch has to be used, increasing the pile up probability. A recent upgrade of the pulser of the Linac gun [27] now allows variation of the pulse duration between 2 and 40 ns, but there is an indication that the bunch width can be extended up to about 200ns (with some compromise with the energy spread and with the power).

The aim of this paper is to identify the best detector and beam conditions to exploit the discovery potential provided by the DAΦNE linac.

4 Experimental technique

The experiment aims to search for the production of a U boson in the process

$$e^+e^- \to U\gamma, \tag{5}$$

where the positrons are the beam particles and e^- are the electrons in the target. The accompanying photon is then detected by a calorimeter regardless of the U decay products. A single kinematic variable characterizing the process, the missing mass, is computed using the formula:

$$M_{miss}^2 = (P_{e^-} + P_{beam} - P_\gamma)^2. \tag{6}$$

Its distribution should peak at M_U^2 for U boson decays, at zero for the concurrent $e^+e^- \to \gamma\gamma$ process, and should be smooth for the remaining background. The approach described provides sensitivity for both visible and invisible searches.

The proposed experimental setup uses the BTF positron beam impinging on a thin target and is composed of the following parts:

- **Active target**, to measure the average position of the beam during a single BTF spill

- **Spectrometer**, to measure the charged interaction products in a given momentum range

- **Dipole magnet**, to deflect the primary positron beam out of the spectrometer and calorimeter and to allow momentum analysis.

- **Vacuum chamber**, to minimize the unwanted interactions of primary and secondary particles.

- **Electromagnetic calorimeter**, to measure and/or veto final state photons.

A schematic view of the experimental apparatus is shown in Figure 5.

The primary beam crosses the target and if a beam particle does not interact it is bent by the magnet to pass between the end of the spectrometer and the calorimeter, thus leaving the experiment undetected. If any kind of interaction causes the positron to lose more than 50 MeV of energy the magnet bends it into the spectrometer acceptance, thus improving the veto capabilities
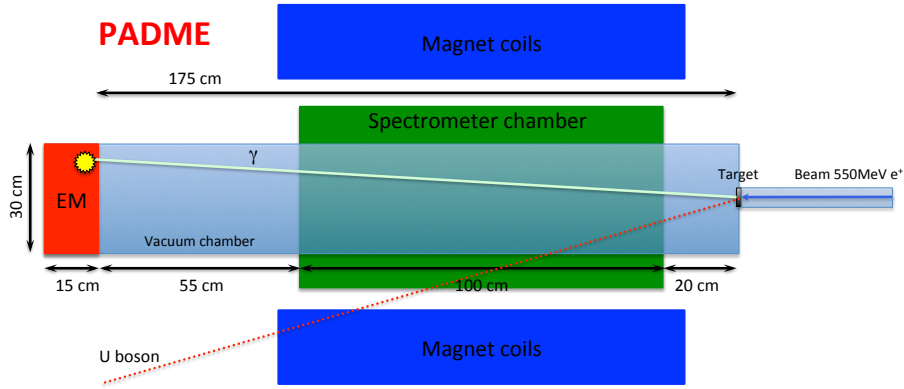
Figure 5: Schematic of the Positron Annihilation into Dark Matter Experiment (PADME).

against background. If a U boson decays into e^+e^- the tracks are also detected by the spectrometer. This could be used to improve the sensitivity in the visible searches.

Due to the very thin target the majority of beam does not interact and can be reused for detector testing provided that appropriate beam optics are built. The proposed experiment is compatible with any activity in the DAΦNE ring, which only results in a reduction of the number of positrons delivered, due to injection of some bunches in the ring.

4.1 U Boson production at BTF

The possible U boson production mechanisms accessible in e^+-on-target collisions are $e^+e^- \to U\gamma$ and $e^+A \to e^+AU$, the so called annihilation and U-strahlung production:
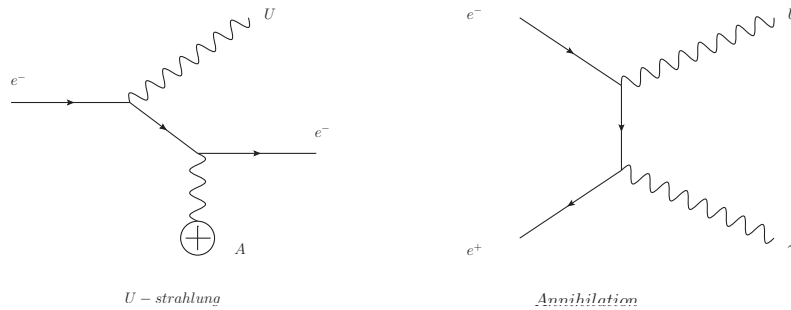
Figure 6: U boson production mechanisms.

Both process are similar to the ones for ordinary photons, as shown in Figure 6, and their cross section scales with ϵ^2. The kinematical constraints given by the well defined centre-of-mass energy in annihilation production is of great importance in rejecting the background and in this paper we will focus our attention on detecting U bosons produced by this mechanism. The present Linac maximum positron energy of 550 MeV allows the production of U bosons through annihilation up to a centre of mass energy of 23.7 MeV. At the same time U bosons with a mass up to the maximum beam energy are produced by U-strahlung. In this case, the cross section scales with $1/M_U^2$ and according to [28] the cross section is proportional to:

$$\sigma(e^+A \to e^+AU) \sim 10^{14} \left(\epsilon \cdot \frac{1MeV}{M_U} \right)^2 \ [pb] \tag{7}$$

7

For the region of parameters under investigation, $M_U \sim 10$ MeV and $\epsilon \sim 10^{-3}$, the expected cross section could be as high as a microbarn.

The cross sections for annihilation and bremsstrahlung emission of an ordinary photon with energy above 1 MeV for positrons on a carbon target are shown in Figure 7. The annihilation cross section was calculated directly with CalcHEP and was compared with the Heitler formula implemented in GEANT4[29]. Agreement within 15% is observed. For the bremsstrahlung the GEANT4 parametrization of the cross section was used.
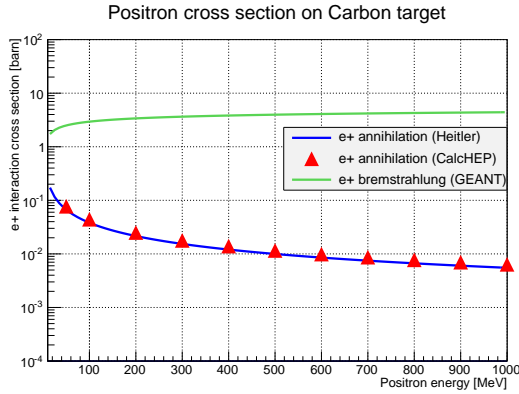
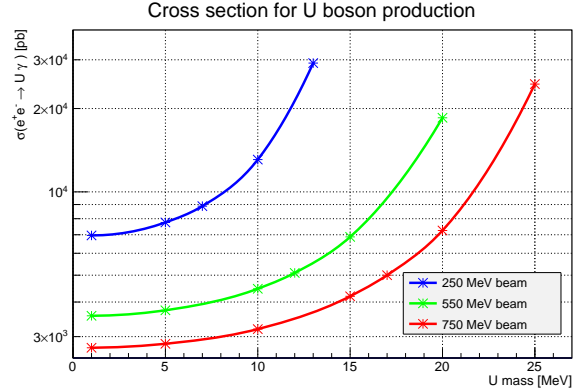Figure 7: *Positron cross section on a carbon target.*

Figure 8: *U boson production cross section as a function of mass for different beam energies*

Since the ratio of annihilation to bremsstrahlung cross sections is proportional to $1/Z$, the lower the Z of the target the better. However due to the requirement to form a rigid and self supporting structure, carbon was chosen as a material. Changing from carbon to silicon worsens the annihilation/bremsstrahlung ratio from $2.3 * 10^{-3}$ ($5.1 * 10^{-3}$) to $1.2 * 10^{-3}$ ($2.7 * 10^{-3}$) for 550 MeV (250 MeV) positrons. The cross section for annihilation of positrons with energies of 550 MeV (250 MeV) is 1.5 mb (3 mb) per free electron leading to a probability of $6 * 10^{-6}$ ($1.2 * 10^{-5}$) in a 50 μm thick carbon target.

Operating the beam line in the regime of $10^4 - 10^5$ e^+ per bunch and 50 bunch/s in one year of data taking with 60% efficiency, a sample of $\sim 10^{13} - 10^{14}$ positrons on target can be collected, corresponding to $\sim (6 \cdot 10^7 - 6 \cdot 10^8)$ annihilation per year. In a zero background experiment, a limit down to $10^{-8} - 10^{-9}$ in ϵ^2 could be set.

Another advantage of the U-annihilation production process comes from the enhancement of the U boson production cross section due to resonant production. As shown in Figure 8, for different beam energies, the production cross section rises fast when the mass of the U boson approaches the available CM energy. The ratio of the the annihilation to bremsstrahlung cross section also increases with the decrease of beam energy, giving an additional rise to the production of the U-boson. This can be exploited by an experiment at the the BTF beam line due to its variable beam energy and could enhance the sensitivity to low-mass U-bosons.

4.2 Active target

Scattering inside the target material worsens the knowledge of the momentum and direction of the primary beam and broadens the reconstructed missing mass spectrum. In fact, in the invisible searches the kinematics cannot be closed without assumptions on the decay vertex and beam direction, while in the visible searches, the vertex position helps in rejecting fake tracks. For this
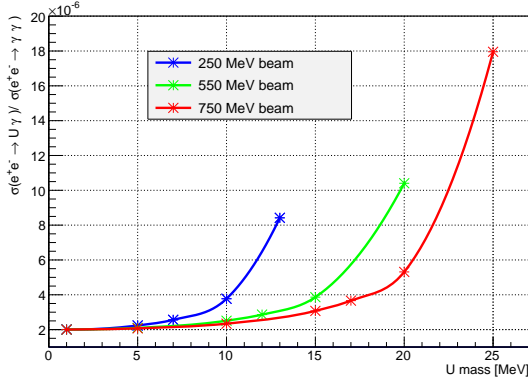
Figure 9: *Ratio of the U boson production and two photon annihilation cross section as a function of the U boson mass for different beam energies*
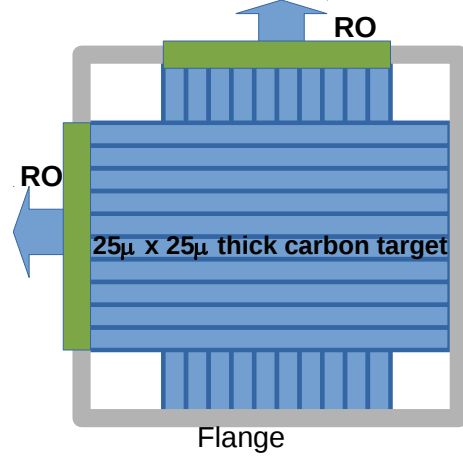

Figure 10: Schematics of the beam monitor

reason the usage of $50\mu m$ target is proposed, for which the simulation showed that the relation $E_{\gamma,brems} + E_{e+} = E_{Beam}$ is fulfilled with a resolution better than the initial beam spread (1%). In addition, the probability of a single annihilation is $\sim$5% per bunch with $\sim 10^4$ positrons.
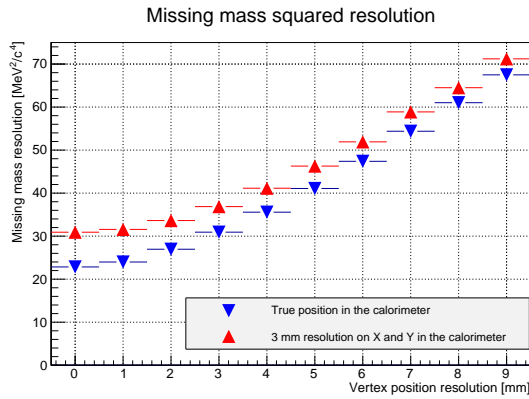

Figure 11: *Dependence of the missing mass squared resolution on the vertex position resolution for a U-boson with $M_U = 15 MeV$.*
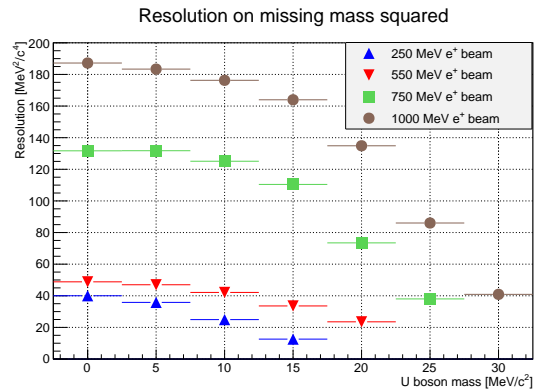

Figure 12: *Missing mass resolution as a function of the U-boson mass for four different energies of the impinging positron beam*

The importance of the beam position measurement can be seen in Figure 11, where the missing mass resolution for a U boson with mass 15 MeV, assuming perfect calorimeter positioning and a realistic 3mm resolution on the cluster position inside the calorimeter, is shown. In order to obtain missing mass resolution down to $\sim 30 MeV^2/c^4$ it is necessary to provide better than 2mm position resolution on the beam spot on the target, which is used for the calculation of the angle of the emitted photon. A single BTF bunch features such a small spot, but due to hysteresis and stability of the currents in the magnets, it is difficult to achieve long term positioning stability better than 5 mm [30].

The design of the proposed target, shown schematically in Figure 10, consist of two orthogonal

9

layers of ten strips made of carbon, each with dimensions 2 mm $\times$ 50 mm $\times$ 25 μm, mounted on a vacuum flange. Both diamond and graphite could possibly be used due to their tolerance to radiation damage and good heat conductivity. The latter is necessary to avoid having to use a cooling system while operating in high intensity beams.

The target will also act as a beam monitor detector, providing the beam spot position bunch per bunch. Its readout will be based on measurement of the secondary electron emission (graphite) or Cherenkov light (diamond). By reconstruction of the beam spot, the uncertainty on the beam geometry will be reduced to that of only a single bunch. An online, two-dimensional beam image would also be useful to optimize the beam parameters while setting up the beam. In addition, it can also be used to measure the number of particles per bunch for intensities of $< 10^5$ positron/bunch, at which methods based on induced current start to be ineffective.

4.3 The dipole magnet

After crossing the active target the charged remnants of the primary beam will be swept away by a sweeping magnet. Because the target is very thin, most of the beam particles will remain in the beam, in the worst case with slightly degraded energy. Due to the low energy of the beam and relaxed spatial constraints, the magnet can be a conventional one. Geant4 simulations show that a magnetic field of ∼0.6 Tesla is enough to deflect the primary 550 MeV beam out of the calorimeter acceptance while keeping most of the electrons from U boson decays inside of the spectrometer acceptance. The magnet surrounds the vacuum region and contains the whole tracking detector, thus serving as a spectrometer magnet. A gap of 50 cm between the coils and a uniform field of length 1 m is assumed.

4.4 The spectrometer

A tracking detector inside the magnetic field will be used to detect charged interaction products and to measure their momentum. The proposed detector is a cylindrical chamber with 5 active layers with a total size of 1m length, 20 cm inner radius and 25 cm outer radius. The chamber is expected to measure the coordinates of a crossing track with a precision of $300\mu m$ in each layer. The size of the spectrometer is defined by the condition that it should detect charged particles with momentum from 50 MeV to 500 MeV travelling along the beam axis, and a positron with $\vec{p} = 550$ MeV should be deflected outside its acceptance. In order to avoid conversion of radiated photons the inner radius should be larger than 20 cm.

4.5 The decay chamber

Due to the high intensity of the beam and the extremely thin target (0.04% X_0), e^+ interactions in air can produce a significant contribution to the background. In fact, since the radiation length of air is 285 m at a pressure of 1013 mbar and the distance from the calorimeter to the target is ∼ 2 m, the atmospheric air thickness is $0.7\% X_0$, which is much larger than the thickness of the target itself.

An MC simulation performed with 1 mbar pressure showed a significant increase in the background with respect to an experiment in vacuum. In interactions in the residual air, the kinematical constraints (i.e. from missing mass) are weakened since the information on the interaction position and the initial beam momentum is completely lost. In addition, the emitted bremsstrahlung photons do not travel through the central calorimeter hole. For the same reason, beam particles not interacting in the target must be transported in vacuum to the dump. Due to the fact that the spectrometer itself contains gas and will not intercept the primary beam, it can be placed outside

the vacuum region. A vacuum with pressure 10^{-1} mbar was chosen for the experiment, which makes the background contribution from beam-air interactions negligible.

4.6 The electromagnetic calorimeter

The electromagnetic calorimeter is responsible for the reconstruction of the photon 4-momentum. An energy resolution of better than $\sim 5\%$ for photons with energies down to 100 MeV and a cluster position resolution of 3 mm are needed in order to achieve squared missing mass resolution of 30 MeV^2/c^4. In addition, a compact shower development is desired to minimize overlapping of signal and background photon clusters.

To achieve such performance, a highly-segmented, inorganic crystal calorimeter made of LYSO was chosen due to its characteristics, listed in Table 2. LYSO has high density, very short X_0 and small Moliere radius together with high light output and short decay time. The calorimeter is an approximate cylinder with a diameter of 30 cm and depth of 15 cm filled with 1x1x15 cm^3 crystals with a round shaped central hole of 4 cm radius, as shown in Figure 13. The active volume will be 9840 cm^3 for a total of 656 crystals. Resolutions down to

$$\sigma_E/E = \frac{1.1\%}{\sqrt{E}} \oplus \frac{0.4\%}{E} \oplus 1.2\% \tag{8}$$

have been recently obtained in the R&D for the calorimeter of the SuperB project in tests with LYSO crystals at the BTF [30] .
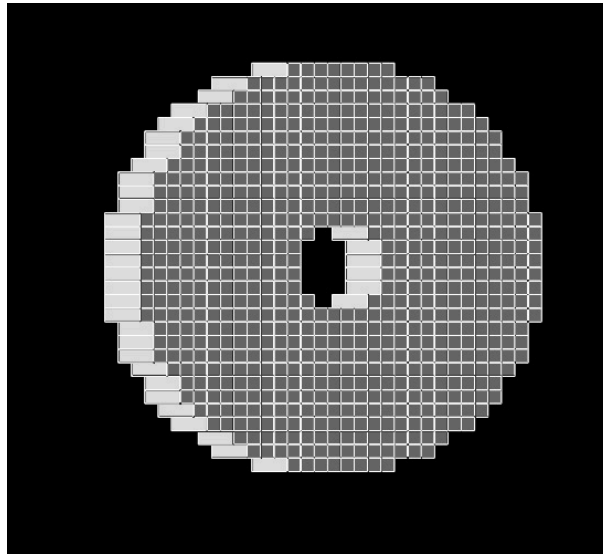

Figure 13: GEANT4 model of the EM calorimeter.

The high segmentation of the electromagnetic calorimeter in the plane transverse to the beam direction assures a spatial resolution of $1/\sqrt{12} = 3$ mm which is equivalent to an angular resolution at 1.75 m from the target below 2 mrad. Energy and angular resolutions obtained with a GEANT4 simulation are in agreement with the performance described above.

5 MC simulation and reconstruction

To understand the actual sensitivity of the proposed experiment to U bosons, a full GEANT4 simulation has been developped. The simulation describes in detail the segmentation of the calorimeter

Density	X_0 (cm)	R_M (cm)	$\tau(ns)$	λ_{peak}	L.Y.	dY/dT(%/C)
7.40	1.14	2.07	40	402	85%	0.2

Table 2: Main parameters of the LYSO(Ce) crystals

and produces energy deposits for each single crystal. The magnetic field is considered to be uniform and transverse to the beam direction. The spectrometer is modelled as an active volume from which the energy of the crossing particles is retrieved without any reconstruction. The simulation does not include any passive material and does not simulate the dumping of the primary beam.

To describe the bunch structure, a simultaneous multi-positron gun was implemented, taking into account beam spot size and energy spread in each single burst. The simulation uses the GEANT4 low-energy electromagnetic libraries. A custom generator was used to simulate the production of the U-boson and its decay into e^+e^-, assuming this to be the unique decay mode. The physical properties (lifetime and decay kinematics) of the U boson were made dependent on two external parameters, allowing the change of the acceptance for different U-boson decay points to be studied. A complete mass scan was performed.

A cluster reconstruction algorithm providing energy and position was implemented, starting from the energy deposits in each of the calorimeter crystals. Initially, a seed crystal is identified, defined as the one with the maximum energy among all the cells in the calorimeter. A seed is created only if the energy is greater than 10 MeV to reject clusters from low energy radiated photons. This condition does not introduce inefficiency in reconstructing photons from U boson production in the mass region under study. The cluster is built by summing the energy of all the crystals with $E > 0.1 MeV$ and distance less than 4.6 cm from the seed, corresponding to 2.5 Moliere radii. All the cells contributing to the cluster are then excluded and the algorithm is repeated until no seed is found. The cluster position is computed by the energy weighted average of the central positions of the cells involved. Due to the relatively high number of cells involved (up to ~40-50) and the small crystal size a spatial resolution as low as 3 mm is achieved. The efficiency for cluster reconstruction is ~ 98%. The present algorithm is not very robust against overlapping clusters but is suitable for the purposes of this analysis.

6   Analysis strategy

A natural choice of a channel for the U-boson production rate normalization is the $e^+e^- \to \gamma\gamma$ channel. The U boson coupling constant can be determined using the formula

$$\frac{\sigma(e^+e^- \to U\gamma)}{\sigma(e^+e^- \to \gamma\gamma)} = \frac{N(U\gamma)}{N(\gamma\gamma)} * \frac{Acc(\gamma\gamma)}{Acc(U\gamma)} = \epsilon^2 * \delta, \tag{9}$$

where $N(U\gamma) = N(U\gamma)_{obs} - N(U\gamma)_{bkg}$ is the number of the signal candidates after the background subtraction, $N(\gamma\gamma)$ is the number of observed annihilation events, δ is the $e^+e^- \to U\gamma$ cross section enhancement factor, as described in Figure 9, and $Acc(\gamma\gamma)$ and $Acc(U\gamma)$ are the corresponding acceptances for the signal and normalization channels.

The U boson sensitivity is limited by the single-photon background, and both, bremsstrahlung and annihilation are potential background candidates.

Bremsstrahlung, the process with higher cross section leads to production of many low energy photons emitted mostly at small angles. For carbon target and 550 MeV beam energy, about 5×10^2 photons with energy > 1 MeV can be produced for each annihilation interaction (see Figure 7).
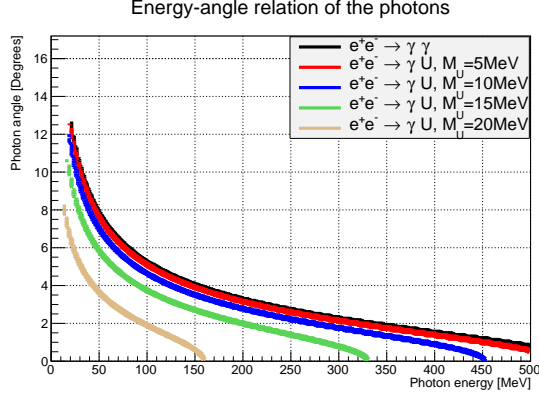
Figure 14: *Gamma energy versus the opening angle for $e^+e^- \to \gamma\gamma$ or $\to U\gamma$ for different U boson masses. Beam energy is 550 MeV*
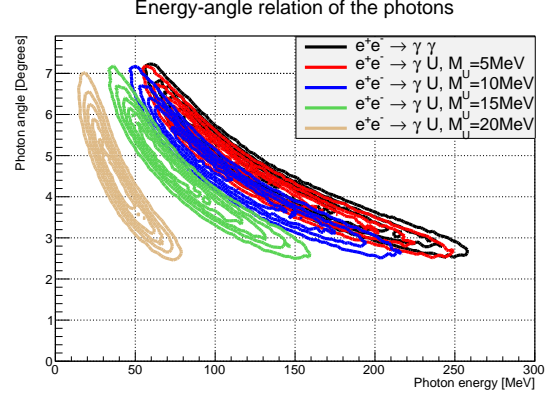

Figure 15: *Gamma energy versus the opening angle after taking into account the geometry and the resolution of the calorimeter and of the vertex position*

The calorimeter has a central hole with an aperture of 1.5 degrees minimizing the sensitivity to most of these photons. The remaining ones populate the entire plain of angle versus energy (see Figure 16) peaking at low energies and low angles.

Because of the closed kinematics the energy and the angle of the annihilation photons are correlated. Due to detector resolution the kinematical region allowed for annihilation photons overlaps that for a low mass U boson (see Fig.14 and Fig.15). To reduce background of this type, a veto on extra clusters in the calorimeter is applied, thus minimizing the contribution from $\gamma\gamma$ final state. The energies of photons produced by synchrotron radiation are very low, at most reaching the hard X-ray region ($\sim$10 KeV). Nevertheless the deflection of the intense beam can give rise to several thousand of these photons, slightly worsening the calorimeter energy resolution.

The missing mass is calculated according to formula (6), with the target electrons assumed to be at rest ($\vec{P}_{e^-} = \vec{0}$) while for the beam a nominal momentum of 550 MeV along the Z axis is used. The signal region is defined as $\pm\sigma_{M^2_{miss}}$ around the reconstructed value of M^2_U, with resolution $\sigma_{M^2_{miss}}(M_U)$ shown in Figure 12.
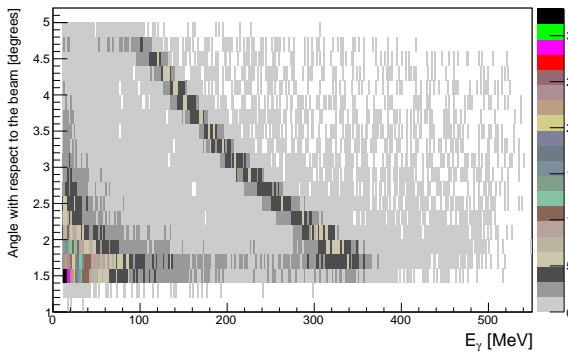

Figure 16: Reconstructed E_γ versus θ distribution for background events.
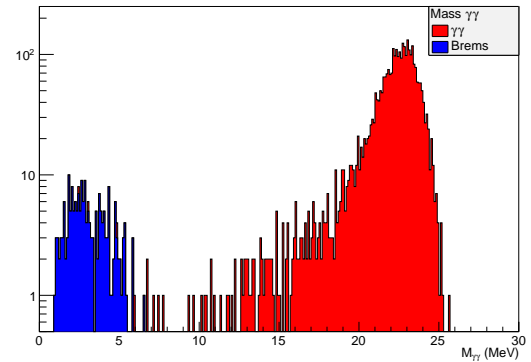

Figure 17: $M_{\gamma\gamma}$ mass distribution.

13

6.1   Signal selection criteria

The selection for U-boson candidates is designed to reject background events as much as possible while keeping the acceptance for U-bosons high. In bremsstrahlung events, the sum of the energies of the positron track and the cluster should be equal to the beam energy since the target is very thin. In $\gamma\gamma$ events the final state has only two clusters and the sum of their energies is equal to the beam energy. The background for a U boson of given mass is estimated by applying the signal selection cuts to the e^+-on-target MC sample and counting the number of events in the signal region.

The selection cuts applied are the following:

- Only one cluster in the calorimeter. This cut rejects most of the annihilation events.

- Cluster energy within $E_{min}(M_U) < E_{Cl} < 400$ MeV. The energy cut is intended to reject low-energy photons from bremsstrahlung radiation and to define a maximum energy of the positron in the spectrometer acceptance to avoid pile up. The energy spectrum of the recoil photons is different for different U masses, resulting in $E_{min}(M_U)$ varying over the interval 50-150 MeV.

- Cluster radius in the calorimeter 5 cm $< R_{Cl} < 13$ cm. This cut reduces the energy leakage and improves M_{miss}^2 resolution.

- Positron veto in the spectrometer. The positron veto cut aims to completely reject the bremsstrahlung gamma by detecting the beam positron inside the spectrometer. Due to the requirement of $E_\gamma > 50$ MeV, the positron is deflected out of the beam by the magnet, enters the acceptance of the tracker and is detected. The veto condition must not reject decays of U bosons, in which a positron is always present. In case a positron with energy below 500 MeV is detected, $E_{e+} + E_\gamma$ has to be lower than 500 MeV. In the U boson case this cut is equivalent to the soft requirement that the electron energy is higher than 50 MeV. This does not play any role in case of invisible U boson decay.

With this selection, an acceptance of $\sim 20\%$ is achieved for U boson mass up to 20MeV.

6.2   Positron flux measurement

The total number of annihilation events $(N(\gamma\gamma)/Acc(\gamma\gamma))$, which are used for normalization, can be determined in two independent ways. The first is to exploit the active target for the measurement of the beam flux and use the known value of $\sigma_{e^+e^-\to\gamma\gamma}$. The signal produced by the active target is proportional to the number of positrons crossing the target itself. Its calibration can be performed by shooting the beam directly onto the calorimeter through the target, measuring the energy deposit and comparing it with the signal from the active target.

Using this curve the number of primary positrons, and therefore the total flux, can be measured in each single bunch. Then the number of annihilations can be calculated as

$$N_{\gamma\gamma}^{tot} = \frac{N_{\gamma\gamma}}{Acc_{\gamma\gamma}} = Flux(e^+) \cdot \sigma_{\gamma\gamma}, \tag{10}$$

since the cross section for the annihilation process ($\sigma_{\gamma\gamma}$) is known with very good precision (Figure 7).

Alternatively, direct reconstruction of the $e^+e^- \to \gamma\gamma$ annihilation events can be performed. For the selection of $\gamma\gamma$ events the same geometrical cuts for signal events are used. Two clusters

in the calorimeter are required, each with reconstructed energy 100 MeV $< E_{Cl} <$ 400 MeV and radius $5cm < R_{Cl} < 13cm$. The $\gamma\gamma$ invariant mass is reconstructed assuming the particles come from the target Z position and using the formula

$$M_{\gamma\gamma} = \frac{\sqrt{[(X_{\gamma 1} - X_{\gamma 2}) + (Y_{\gamma 1} - Y_{\gamma 2})]E_{\gamma 2}E_{\gamma 2}}}{Z_{EMcal} - Z_{Target}}. \tag{11}$$

In Figure 17 the distribution of $M_{\gamma\gamma}$ from MC is shown. The genuine $\gamma\gamma$ events (in red) peak at the centre of mass energy of the e^+e^- pair while the negligible bremsstrahlung background (in blue) is situated at small $M_{\gamma\gamma}$. The expected contamination from bremsstrahlung processes in the signal region is well below the 0.1% level. The resolution on $M_{\gamma\gamma}$ is found to be 1 MeV. Using the GEANT4 simulation and the invariant mass cut 20 MeV $< M_{\gamma\gamma} <$ 26 MeV, the acceptance for this selection has been measured to be $\sim 7\%$, with a calorimeter geometrical acceptance for two photons of $\sim 17\%$. The expected precision in the measurement of the flux is dominated by the value of the annihilation cross section, since the statistical error on $\gamma\gamma$ sample is $\sim$0.05 %.

Combining the two results for the number of primary positrons, the cross section for the annihilation process ($\sigma_{\gamma\gamma}$) can be measured as a by-product. This will help to cross check the reliability of the obtained flux, minimizing the systematics.
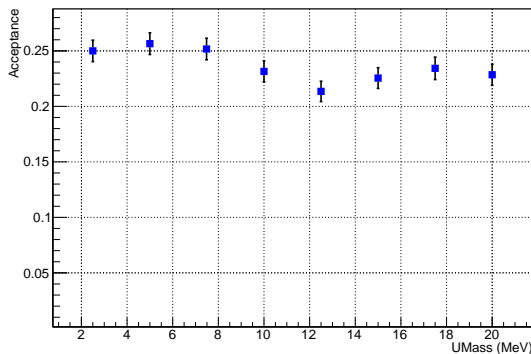
6.3 Sensitivity

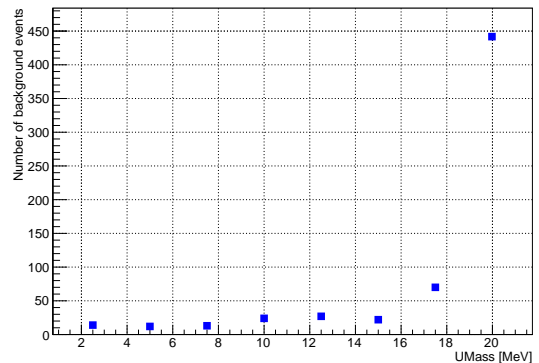Figure 18: *Acceptance for U boson detection as a function of its mass*

Figure 19: *Background contribution as a function of the U boson mass*

With the described experimental setup and simulation technique, 10^7 events were generated, each with 10^4 positrons, corresponding to about 56 hours of running of the DAΦNE linac at full efficiency. In addition, samples of 2000 events were generated for the following values of U-boson masses: 2.5, 5, 7.5, 10, 12.5, 15, 17.5, 20 MeV, with a single U boson produced per bunch with 10^4 positrons. The acceptance (Figure 18) and the expected number of background events (Figure 19) were obtained by running the events through the selection.

The background was further scaled by a constant factor of 100 to account for one year of running of the experiment with 60% efficiency. Under the assumption of no signal, an upper limit on the coupling ϵ can be set, using the statistical uncertainty on the background. The expected exclusion region is shown in Figure 20 and is applicable both to the invisible and visible channels.
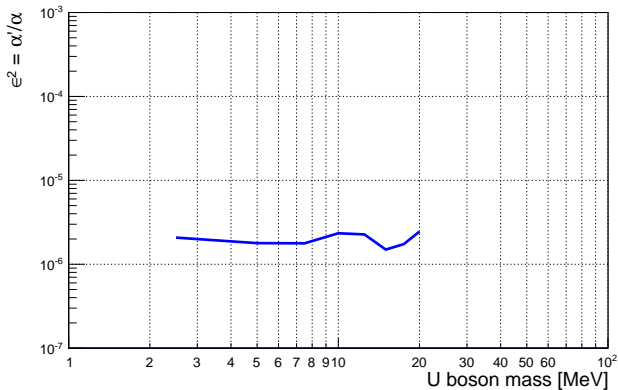
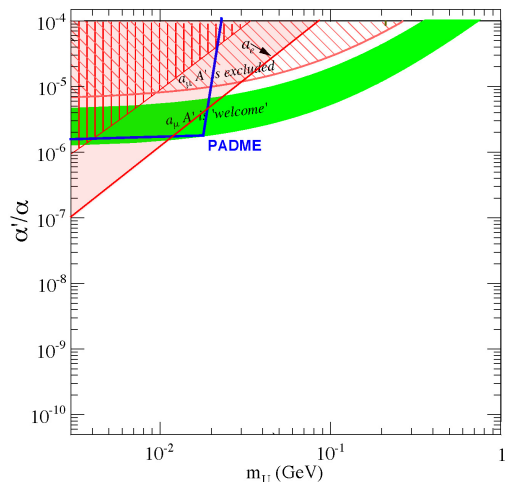Figure 20: Expected exclusion limits in the $\epsilon - M_U$ plane in case of no signal

Figure 21: *Expected exclusions in the invisible channel compared with the band of values preferred by current $g_\mu - 2$ discrepancies.*

7 Conclusions and discussion

Searches for dark photons are well motivated by recently observed phenomena. The analysis presented in this paper shows that such a search can be performed exploiting the present linac of the DAΦNE facility in just one year of running. The expected sensitivity $\epsilon^2 \sim 10^{-6}$ is common both to the visible and invisible U boson decays and lies exactly in the most interesting region, preferred by the $g_\mu - 2$ data, as seen in Figure 21. It partially overlaps with the result of the combination of the measurements of $(g_e - 2)$ and α_{EM}, exploiting tenth-order calculations of the QED contributions. As discussed in section (2), that region is still of high interest since no direct search for a U-boson has been performed accessing it and because of the recent shift by more than 7σ [31] of the theoretical prediction for g_e due to an error in the calculations. The proposed experiment could be the first to constrain the invisible channel. An upgrade of the BTF positron beam energy to 750 MeV will extend the sensitivity to higher U-boson mass.

At present there are a few experiments in different phases of preparations devoted to the search for dark photons - VEPP3 [32], DarkLight [33] and HPS [34]. Among them, only VEPP3 is sensitive to invisible decays in the same region of parameter space. While the general approach is similar, there are few crucial differences. The VEPP3 proposal aims to use a storage ring which limits the beam energy to a fixed value of 500 MeV, while the DAΦNE Linac could be able to provide positrons with variable beam energy from 250 MeV up to 750 MeV and a beam spread of 1%, thus extending the accessible region of U-boson masses. Moreover, the presence of an active target allows the determination of the interaction vertex at the mm level, leading to a reduction of the background through improvement of the missing mass resolution. Another advantage of the experiment proposed in this paper is the relatively small calorimeter, since it is placed at a distance from the target about three times smaller with respect to the VEPP3 one, which minimizes the cost and timescale of the experiment. The presence of a magnetic spectrometer, apart from further reducing the background by measuring the momentum of the positrons that had emitted hard bremsstrahlung photons, could possibly allow the direct study of visible $U \to e^+ e^-$ decays. This channel makes the experiment sensitive to the bremsstrahlung production of U bosons,

16

thus pushing the accessible parameters region to higher masses. While providing an interesting benchmark possibility with the comparison of the results from visible and invisible searches done simultaneously, this falls outside the scope of the present paper and will be a subject of a future study.

Acknowledgments

References

[1] O. Adriani *et al.* [PAMELA Collaboration], Nature **458**, 607 (2009).

[2] M. Ackermann *et al.* [Fermi LAT Collaboration], Phys. Rev. Lett. **108**, 011103 (2012).

[3] M. Aguilar *et al.* [AMS Collaboration], Phys. Rev. Lett. **110**, 141102 (2013).

[4] O. Adriani *et al.* [PAMELA Collaboration], Phys. Rev. Lett. **105**, 121101 (2010).

[5] J. Beringer *et al.* [Particle Data Group], Phys. Rev. D**86**, 010001 (2012).

[6] P. Fayet, Phys. Lett. B **675**, 267 (2009).

[7] B. Holdom, Phys. Lett. B **166**, 196 (1986)
P. Galison and A. Manohar, Phys. Lett. B **136**, 279 (1984).

[8] A.Pukhov *et al.*, Preprint INP MSU 98-41/542,arXiv:hep-ph/9908288
A.Pukhov, e-Print Archive: hep-ph/0412191.

[9] S. Andreas, C. Niebuhr and A. Ringwald, Phys. Rev. D **86**, 095019 (2012).

[10] E. M. Riordan *et al.*, Phys. Rev. Lett. **59**, 755 (1987).

[11] J. D. Bjorken *et al.*, Phys. Rev. D**38**, 3375 (1988).

[12] A. Bross, M. Crisler, S. H. Pordes, J. Volk, S. Errede and J. Wrbanek, Phys. Rev. Lett. **67**, 2942 (1991).

[13] J. Schweppe *et al.*, Phys. Rev. Lett. **51**, 2261 (1983).

[14] H. Merkel *et al.* [A1 Collaboration], Phys. Rev. Lett. **106**, 251802 (2011).

[15] S. Abrahamyan *et al.* [APEX Collaboration], Phys. Rev. Lett. **107**, 191804 (2011).

[16] F. Bossi, Advances in High Energy Physics **2014**, 891820 (2014).

[17] P. Adlarson *et al.* [WASA-at-COSY Collaboration], Phys. Lett. B **726**, 187 (2013).

[18] F. Archilli, D. Babusci, D. Badoni, I. Balwierz, G. Bencivenni, C. Bini, C. Bloise and V. Bocci *et al.*, Phys. Lett. B **706**, 251 (2012).

[19] D. Babusci *et al.*, Phys. Lett. B **720**, 111 (2012).

[20] B. Aubert *et al.* [BaBar Collaboration], Phys. Rev. Lett. **103**, 081803 (2009).

[21] M. Pospelov, Phys. Rev. D **80**, 095002 (2009).

[22] D. Hanneke, S. Fogwell Hoogerheide, and G. Gabrielse, Phys. Rev. A **83**, 052122 (2011).

[23] R. Bouchendira *et al.*, Phys. Rev. Lett. **106**, 080801 (2011).

[24] T. Aoyama *et al.*, Phys. Rev. Lett. **109**, 111807 (2012).

[25] A. Ghigo, G. Mazzitelli, F. Sannibale, P. Valente and G. Vignola, Nucl. Instrum. Meth. A **515**, 524 (2003).

[26] P. Valente, "Possible upgrades of the DAFNE Beam Test Facility", unpublished

[27] B. Buonomo et al., DAFNE note in preparation, (2014).

[28] J. D. Bjorken, R. Essig, P. Schuster and N. Toro, Phys. Rev. D **80**, 075018 (2009).

[29] W. Heitler., The Quantum Theory of Radiation, Clarendon Press, Oxford (1954).

[30] G. Eigen *et al.*, Nucl. Instrum. Meth. A **718**, 107 (2013).

[31] T. Aoyama, M. Hayakawa, T. Kinoshita, and M. Nio, Phys. Rev. Lett. **99**, 110406 (2007).

[32] B. Wojtsekhowski, AIP Conf. Proc. **1160**, 149 (2009), arXiv:0906.5265 [hep-ex]
B. Wojtsekhowski, D. Nikolenko and I. Rachek, arXiv:1207.5089 [hep-ex].

[33] M. Freytsis, G. Ovanesyan and J. Thaler, JHEP **1001**, 111 (2010); [arXiv:0909.2862 [hep-ph]].

[34] The Heavy Photon Search Collaboration (HPS),
https://confluence.slac.stanford.edu/display/hpsg/